THE ENSENADA FRONT: JULY 1985

LOREN R. HAURY, ELIZABETH L. VENRICK,
CONNIE L. FEY, JOHN A. MCGOWAN
Marine Life Research Group
Scripps Institution of Oceanography
University of California, San Diego
9500 Gilman Drive
La Jolla, California 92093-0218

PEARN P. NIILER
Physical Oceanography Research Division
Scripps Institution of Oceanography
University of California, San Diego
9500 Gilman Drive
La Jolla, California 92093-0230

ABSTRACT

The surface signature of the relatively cool, fresh, eutrophic waters of the southeastward-flowing California Current end abruptly off northern Baja California, Mexico, in a persistent, interannually variable feature we call the Ensenada Front. A detailed study of the front in July 1985 showed that it comprised a complex set of flows, some of which fed into eddies and others that may have been subducting under the warm, oligotrophic waters to the south. The frontal region was characterized by low gradients in physical, chemical, and biological properties. The nutricline was about 35 m deep north of the front and 100 m deep south of it. Integrated primary production to the north was three times that to the south; productivity was not enhanced in the jets. Integrated euphotic-zone chlorophyll showed no significant change across the front; an area northeast of the front with a strong, deep chlorophyll maximum (DCM) underlying a pool of warm, low-chlorophyll water had the highest integrated chlorophyll in the study region. Chlorophyll concentrations increased in the high shear zones between strong jets. The highest values of surface chlorophyll and primary production tended to correspond to regions of lowest geopotential anomaly, not to regions of low temperatures and positive divergence. Wet displacement volumes of zooplankton in the upper 210 m were three times higher to the north of the front, and in the upper 100 m were four times higher; the change occurred relatively abruptly over a distance of about 15 km. Zooplankton biomass varied directly with integrated chlorophyll in north-south sections across the southeast-trending front, but varied inversely with chlorophyll on a west-east section that ended in the warm pool with the strong DCM. Fish eggs and larvae were less abundant in the waters north of the front.

RESUMEN

Las aguas superficiales de la corriente de California que fluyen hacia el sureste se caracterizan por ser relativamente eutróficas, frías y menos salinas. Las aguas superficiales cambian abruptamente de características frente al norte de Baja California, México. La zona de cambio, que aquí denominamos el Frente de Ensenada, es persistente y varía de año a año. En Julio de 1985 se realizó un estudio que mostró que el frente estaba formado por un intrincado conjunto de corrientes. Algunas de éstas corrientes alimentaban remolinos, mientras que otras podrían haber estado encajándose bajo aguas tibias y oligotróficas que se encontraban hacia el sur. El frente se caracterizó por gradientes poco intensos en las propiedades físicas, químicas y biológicas. La nutraclina se encontraba a 35 m de profundidad al norte del frente, mientras que al sur, se encontraba a 100 m. Hacia el norte del frente la producción primaria integrada fué tres veces mayor que al sur. La productividad no incrementó en los chorros. La clorofila (integrada para la zona eufótica) no varió significativamente a través del frente. Los valores máximos de clorofila (integrada para la zona eufótica) ocurrieron en una zona al noreste del frente; en ésta zona, se encontró un máximo-profundo de clorofila bajo una parcela de agua tibia (con concentraciones bajas de clorofila). Las concentraciones de clorofila incrementaron en las zonas de mayores gradientes horizontales de velocidad entre los chorros. En general, los valores más altos de clorofila superficial y producción primaria coincidieron con las regiones de menor anomalía geo-potencial y no con las zonas de temperaturas bajas y divergencia positiva. En los 210 m más someros de la columna de agua, el volumen húmedo desplazado de zooplancton fué tres veces mayor al norte del frente; en los 100 m más someros, cuatro veces. Estos cambios ocurrieron con relativa rapidez en una distancia de 15 km. El frente tendía al sureste, y mientras que en transectos norte-sur la biomasa de zooplancton varió directamente con la clorofila integrada, la variación fué inversa en un transecto oeste-este. Al final de éste último transecto fué cuando se encontró la parcela de agua tibia con un elevado máximo-profundo de clorofila. La abundancia de huevos y larvas de peces fué menor en aguas al norte del frente.

[Manuscript received November 11, 1992.]

INTRODUCTION

It has been known for more than fifty years that the generally southeastward-flowing California Current turns shoreward toward northern Baja California in the vicinity of 32°N (Sverdrup and Fleming 1941; Wyllie 1966; Hickey 1979; Lynn and Simpson 1987; Pares-Sierra and O'Brien 1989). Some of the onshore flow turns north to form part of the cyclonic Southern California Eddy and Southern California Countercurrent (Jackson 1986); the remainder turns southward along the northern Baja California coast. The shoreward flow is also associated with a broad faunal boundary between pelagic organisms of northern (cool eutrophic water) and southern (warm oligotrophic water) affinities (e.g., Brinton 1976; Sette and Ahlstrom 1948).

Only within the last fifteen years, however, has the detailed physical and biological structure of this flow begun to be resolved. Satellite infrared images from 1975 and 1976 showed a recurring oceanic frontal zone in the region (Bernstein et al. 1977; Legeckis 1978) and Coastal Zone Color Scanner (CZCS) imagery showed a persistent, interannually variable front in chlorophyll between 1979 and 1982 (Pelaez and McGowan 1986; Thomas and Strubb 1990). The front is detectable much of the year, but is most strongly developed from late March to early June. The surface expression of the northern California eutrophic waters disappears in the frontal region, but the water parcels continue moving southward. The considerable warming and loss of surface pigment occurs rapidly perpendicular to, and along the path of, the frontal flow.

Niiler et al. (1989) studied the three-dimensional mesoscale physical dynamics of the flow associated with the front. They showed the presence of a narrow (about 50 km), surface-intensified jet to at least 300 m, with velocities in excess of 25 cm s^{-1}; the core of the flow had upwelling estimated to be about 50 cm day^{-1}. They also suggested that the abrupt disappearance of the cold, pigment-rich water along the front is due in part to subduction of these waters to the southwest. Chereskin and Niiler[1] describe in more detail similar circulation features observed in the frontal region in September 1988.

Thomas and Strub (1990) used the CZCS West Coast Time Series (1979–83 and 1986) to describe in more detail the seasonal and interannual temporal and spatial variability of the front's phytoplankton pigment signature. Seasonality in pigment concentration is weak to the south and strong to the north. In the north, pigments have two peaks—in late spring and early fall. High pigment concentrations extend farther offshore (150–300 km) in the spring and early summer than in the mid to late summer. Interannual variability in latitudinal position of the front was about 150 km. In June of El Niño year 1983, the front was detectable for only a short time.

In this report we describe the physical, chemical, and biological characteristics of this front off northern Baja California, Mexico, using data collected during and shortly after the period of Niiler et al.'s (1989) synoptic study of the shoreward flow and mesoscale features of the front. The front has been called the East Pacific Subtropical Front (Legeckis 1978), a name which has also been applied to a more oceanic feature (e.g., Saur 1980; Lynn 1986). To avoid confusion we have called this feature the Ensenada Front (Haury et al. 1990; Venrick 1990) in recognition of its geographical location.

METHODS

The data were collected from 1 to 23 July 1985 on the two legs of the FRONTS 85 cruise on RV *New Horizon*; the ship track and station positions for Leg I are shown in figure 1a. The sampling pattern was located on the basis of an AVHRR satellite image received on the first day of the leg and modified as *in situ* data became available. During the second leg, cloud cover precluded further use of satellite imagery; hence the station plan was oriented according to the earlier images and Leg I information. Three replicate north-south (N-S) transects were made across the front followed by a west-to-east (W-E) section (figure 1b). On either side of the front at the ends of each N-S transect, a 24-hour station was occupied on each of two days, four days apart. Replicate observations made at these stations allowed characterization of the two types of water constituting the front, and of small-scale heterogeneity within the two types.

Details of most of the sampling methods, data handling, and accuracies are presented in Haury et al. 1986, with additional information in Niiler et al. 1989; the following is a summary of these techniques and others not previously described. Leg I data consisted of 81 Neil Brown CTD lowerings to 300 or 500 m, 90 XBT drops, 20 ARGOS-tracked drifters drogued at 15 m (Niiler et al. 1987) deployed at CTD stations from 8 to 10 July, and 8 hydrocasts collecting water at six depths to measure chlorophyll and primary production (^{14}C incubation, noon to sunset). The ship's uncontaminated seawater system was used for underway measurements of 3-m tem-

[1]Chereskin, T. K., and P. P. Niiler. Circulation in the Ensenada Front: September 1988. MS submitted to Deep-Sea Res.

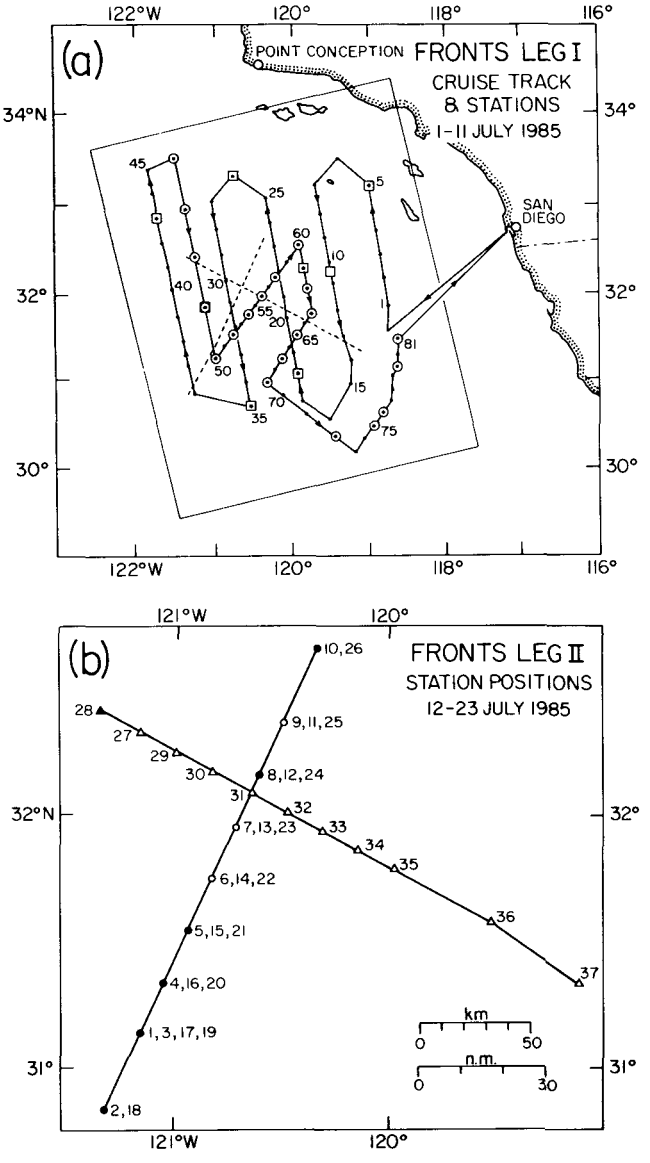

Figure 1. *a*, Cruise track and station positions for FRONTS 85 Leg I. *Small black dots* indicate CTD casts; *circled dots*, ARGOS-tracked drifter deployments; *squares*, primary productivity measurements. The boxed area denotes the region studied and illustrated in Niiler et al. 1989 and used in figure 4. The *dashed lines* indicate the transects detailed in *b*, which shows the station positions for FRONTS 85 Leg II, numbered by order of occupation. *Filled circles* and *triangles* indicate stations where at least one measurement of primary productivity was made.

perature and chlorophyll fluorescence at 5-minute intervals.

Leg II data were obtained from 40 hydrocasts with 20 Nansen bottles to a maximum depth of 1000 m. Temperature, salinity, oxygen, and nutrients were determined from all depths sampled; chlorophyll and phaeopigments were determined from the top 12 depths. Nine casts for primary production and underway temperature and chlorophyll data were collected as during Leg I. One or more macrozooplankton samples were obtained at each station during Leg II (54 total) with oblique bongo net tows to 210 m using the standard CalCOFI procedures described in Kramer et al. (1972).

A twenty-net MOCNESS system (1-m^2 mouth, 333-μm mesh; Wiebe et al. 1985) was used to take replicate samples of day and night vertical distributions of macrozooplankton at the ends of the N-S sections. Wet displacement volume measurements (after removal of organisms >5 ml) of all macrozooplankton samples are presented here, together with counts of fish eggs and larvae, provided courtesy of G. Moser, NOAA NMFS Southwest Fisheries Science Center, La Jolla. Moser and Smith (in press) describe in detail the taxonomic composition, abundance, and distribution of fish larvae. The data presented here for the bongo net tows combine the average values from the two sides. Night-to-day ratios of the bongo net macrozooplankton displacement volumes and counts of fish eggs and larvae (based on 29 daytime samples and 25 night samples) were 1.4 for eggs, and 1.6 for larvae. These ratios have been applied as a correction to the daytime samples for graphing and further analysis.

RESULTS

Physical Structure and Dynamics

AVHRR imagery from 1 July (figure 2) showed the Ensenada Front in the survey area as a sinuous

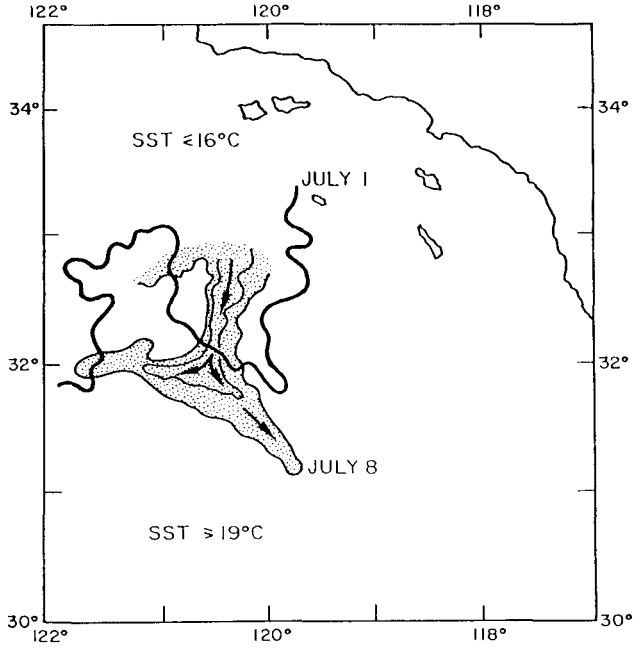

Figure 2. The location of the main gradient of sea-surface temperature, indicative of the Ensenada Front, on 1 July (*heavy black line*) and 8 July (*thin black line*) 1985. The frontal shapes were traced from AVHRR images; the arrows denote flow after 8 July as indicated by drifter tracks (see figure 3).

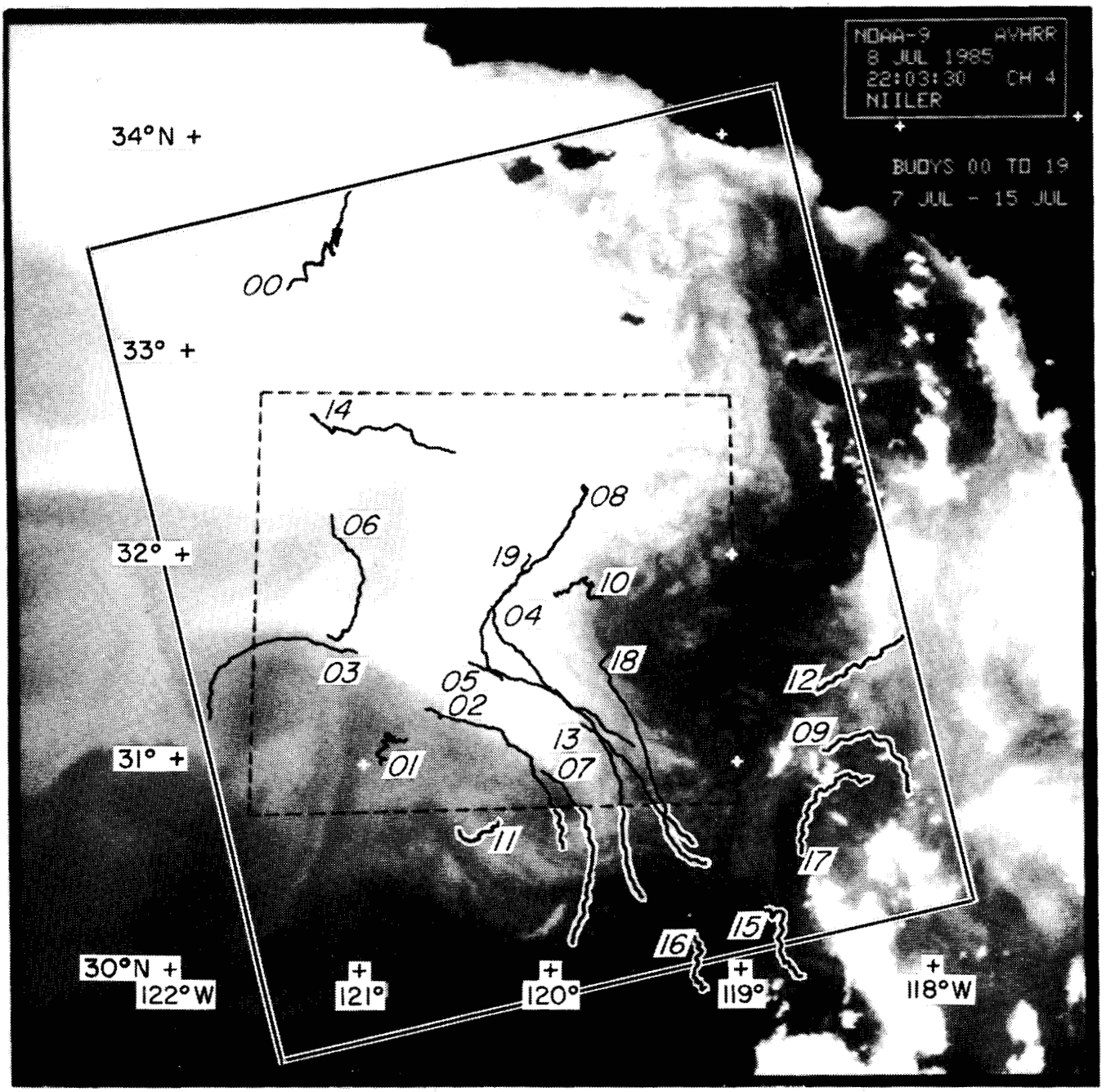

Figure 3. Satellite infrared image of the California Current system south of Point Conception taken on 8 July 1985 at 2204 UT. Light grey shades correspond to relatively cold water. Drifter tracks, numbered at launch site, from deployment time through 15 July are overlaid in black. The *solid and dashed boxes* denote the study area shown in figure 1a and the location of the transects shown in figure 1b. Adapted from Niiler et al. 1989.

southwest-to-northeast-trending boundary between cold (<16°C) and warm (>19°C) water. By 8 July, the southward-extending tongue of cold water forming the eastern portion of the front had evolved into an anvil-shaped structure (figures 2 and 3) with most of the flow turning eastward, as indicated by the drifter tracks (figure 3). The continuation of the front to the west of this diverging flow was oriented generally to the northwest, extending out of our survey area. Another tongue of cold water flowed westward from this region, seen as the band of cool water at 32°30′N on the left side of figure 3. This water fed the eddy dipole system described by Simpson and Lynn (1990); the eastern half of both these eddies can be seen on either side of the cold water in figure 3. Plate 1 of Simpson and Lynn

(1990), using larger-scale AVHRR images, shows all of these mesoscale structures and traces the development of the flow along the front between 1 and 9 July 1985.

The study of Niiler et al. (1989) summarized in the introduction is augmented here with other shipboard observations. The geopotential anomaly (15/300 db) mapped from Leg I data (figure 4a) showed the narrow and sinuous nature of the dominating current flow through the study area. Divergence, calculated from the geopotential anomaly and from drifter tracks, is illustrated in figure 4b to indicate the inferred regions of potential upwelling. The surface-temperature manifestations of the flow, as evidenced by the 3-m temperature measured every 5 min (1.54 km) while underway during Leg I, are shown in figure 4c. The maximum gradient observed was 0.36°C km^{-1} near station 28 (figure 1a) in the edge of the warm-water (>19°C) intrusion to the west of the anvil stem. This gradient was the exception, however; the cumulative frequency distribution showed that 75% of all gradients were less than 0.05°C km^{-1}, 90% less than 0.09°C km^{-1}, and 99% less than 0.22°C km^{-1}. The underway measurements made on the four sections of Leg II showed the same small gradients; these results are summarized in table 1. The frontal region, except for a few small areas, was not characterized by sharp temperature gradients. This is very unlike frontal systems nearer shore (Simpson 1985). Despite the low gradients, the region still displayed a complex temperature structure reflecting the underlying physical dynamics (see below).

The surface waters of the filament entering the study area in the northwest corner had a temperature of about 16.5°C, while those exiting the area towards the east (southeast corner) were slightly less than 17.5°C in the core (figure 4c). This suggests that the water warmed by about 1°C as it passed through the area, due to mixing with the surrounding waters and to surface heating.

Three CTD-XBT sections (station spacing 10 km) were made across and normal to the west-to-east-flowing jet during Leg I (stas. 50–60, 63–69, and 73–81; figure 1a). Niiler et al. (1989) illustrate (their figure 8) the temperature, salinity, and geostrophic current relative to 300 db through the first two sections of this onshore-flowing filament. These sections showed a relatively strong thermohaline front at the southern edge; this density structure was responsible for geostrophic velocities as high as 70 cm s^{-1}. The sections also showed a shallow salinity minimum extending southward between 50 and 100 m under the front, confirming the

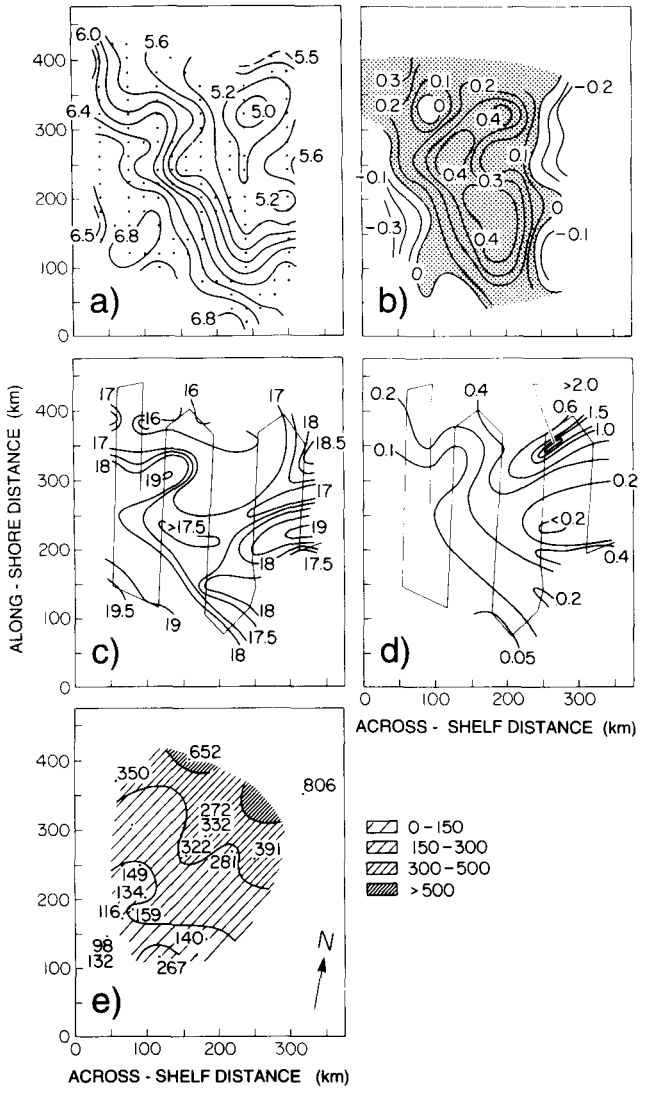

Figure 4. *a*, Objective map of the 15/300 db geopotential anomaly from FRONTS 85 Leg I data. Contour interval is 0.2 m^2 s^{-2}. Station positions after binning are indicated by *dots* (from Niiler et al. 1989, fig. 3). *b*, Geostrophic divergence calculated from the 15/300 db geopotential anomaly. Regions of positive divergence are *stippled*; units are $10^{-7}s^{-1}$ (adapted from figs. 10b and 14b of Niiler et al. 1989). *c*, Temperature (contour intervals 0.5°C) and *d*, chlorophyll *a* (μg l^{-1}) at 3 m measured under way at 5-min intervals (1.5 km) along the portion of the Leg I cruise track shown by the *light straight lines*. e, Primary productivity (mgC m^{-2} exp^{-1} integrated over the euphotic zone) estimated from noon-to-dusk ^{14}C incubations at stations occupied during Leg I and II.

intrusion and subduction of low-salinity water to the southwest. The third, easternmost section showed the flow to have spread and dampened, leaving no evidence of an intense current or subduction.

Figures 5 and 6 present the two geostrophic current sections from Niiler et al. 1989 and the corresponding underway surface data for all three sections to describe in more spatial detail (data points every 1.5 km) the surface structure of the front and the current filaments and the surface structure's relation to deeper features. As expected, the

TABLE 1
Temperature and Chlorophyll Gradients (First Differences; °C km^{-1} and mg m^{-3} km^{-1}) from Underway Measurements[a] during FRONTS 85

	Leg I		Leg II							
			Section 1 stas. 2–10		Section 2 stas. 10–18		Section 3 stas. 18–26		W-E Section stas. 27–37	
	T	Chl	T	Chl	T	Chl	T	Chl	T	Chl
Maximum gradient	0.36	0.14	0.28	0.13	0.27	0.05	0.38	0.06	0.31	0.04
75% less than[b]	0.05	0.01	0.03	0.01	0.06	0.01	0.04	0.01	0.06	0.01
90% less than[b]	0.09	0.02	0.08	0.01	0.10	0.03	0.06	0.03	0.10	0.01
99% less than[b]	0.22	0.09	0.27	0.06	0.16	0.04	0.17	0.06	0.22	0.02

See figure 1 for cruise track and station positions for each leg.
[a]Made at 3-m depth every 5 min (1.5 km)
[b]Percentage of gradients less than table value

underway temperature and salinity data for the first two sections indicated that the highest gradients were associated with the strongest flows. In the first section (figure 5, stas. 50–60), the two coldest temperatures (<17.5°C) were associated with strong southeastward flows and a weak boundary between southeastward and northwestward flows; the very-low-salinity water (<33.4 psu), however, was found only in the strongest southeastward flow. The second section (figure 5, stas. 63–69) had warmer minimum and maximum temperatures, this time with the warmest water to the north of the filament; salinity again was lowest in the strong southern edge of the flow. Although the surface signatures of the two crossings of the filament were similar, the deeper measurements reveal that only the first section had northwest flows; all the second-section flow above 100 m (with respect to 300 db) was to the southeast. The rich detail and relatively large gradients in the underway data for both sections, however, suggest that the structure of the flow is much more complex than indicated by the CTD-XBT sections, with potential consequences for transport and biology (see below). The weakened and dispersed flows of the easternmost section have much lower temperature fluctuations (figure 6; temperature range of 19.1 to 20.3°C), but the same salinity range as the strong-flow sections (33.2 to >33.5 psu), indicating an apparent rapid warming of the advecting water masses.

During FRONTS 85 Leg II, the hydrographic station separation on the N-S sections was 24 km (37 km for the terminal stations), slightly more than the 10 km between alternate CTD and XBT stations of Leg I, so there is less detail in the depth profiles of properties (figures 7–9). The original intention of these transects was to repeat the sections across the strong west-to-east jet as was done on Leg I. The lack of warmer and more saline water on the northern ends of these three transects, satellite imagery evidence of the southeasterly drift in the "stem" of the anvil-shaped flow, and an abrupt salinity front found just to the east of the transects (see below) suggest that the Leg II transects were made down the axis of the southward-flowing "stem" and crossed the front near the point where the flow diverged to the west and east. It is likely, as shown below, that each N-S transect was progressively closer to the center of the cold axis of the N-S filament.

The three sections along the same geographical track illustrate the structure and variability in the system over the week of sampling; the relatively weak gradients shown in the transects (figures 7–9 and table 1) probably resulted from the failure of the sections to cross perpendicular to the high-velocity filaments. Underway surface data obtained as on Leg I, however, showed considerable small-scale (<5 km) variability in the properties (figure 10). Subduction at the front of the low-salinity (<33.3 psu) and cool northern water is clear in the three sections (figure 7). All sections show discontinuities in the layer of minimum salinity at the vicinity of the front between 31.5° and 32°N; whether this is a result of undersampling, episodic subduction, or variability in the properties of the southward-flowing water cannot be determined.

The reduction in more-saline (≥33.4 psu) water with time (figure 7) indicates the advection of the southward-flowing stem to the southeast. In view of this possible advection, a remarkable feature of the geostrophic velocity sections (figure 7) is the consistency displayed in the location and intensity of the westerly flows over a period of almost 7 days. The northern region of westerly flow (stas. 8–9, 11–12, 23–24) was probably associated with a meander of the strong southerly flow of the filament. The southern region of westerly flow (stas. 3–4, 16–17, 19–20) perhaps was associated with entrainment of waters into the northern limb of the eddy (center at

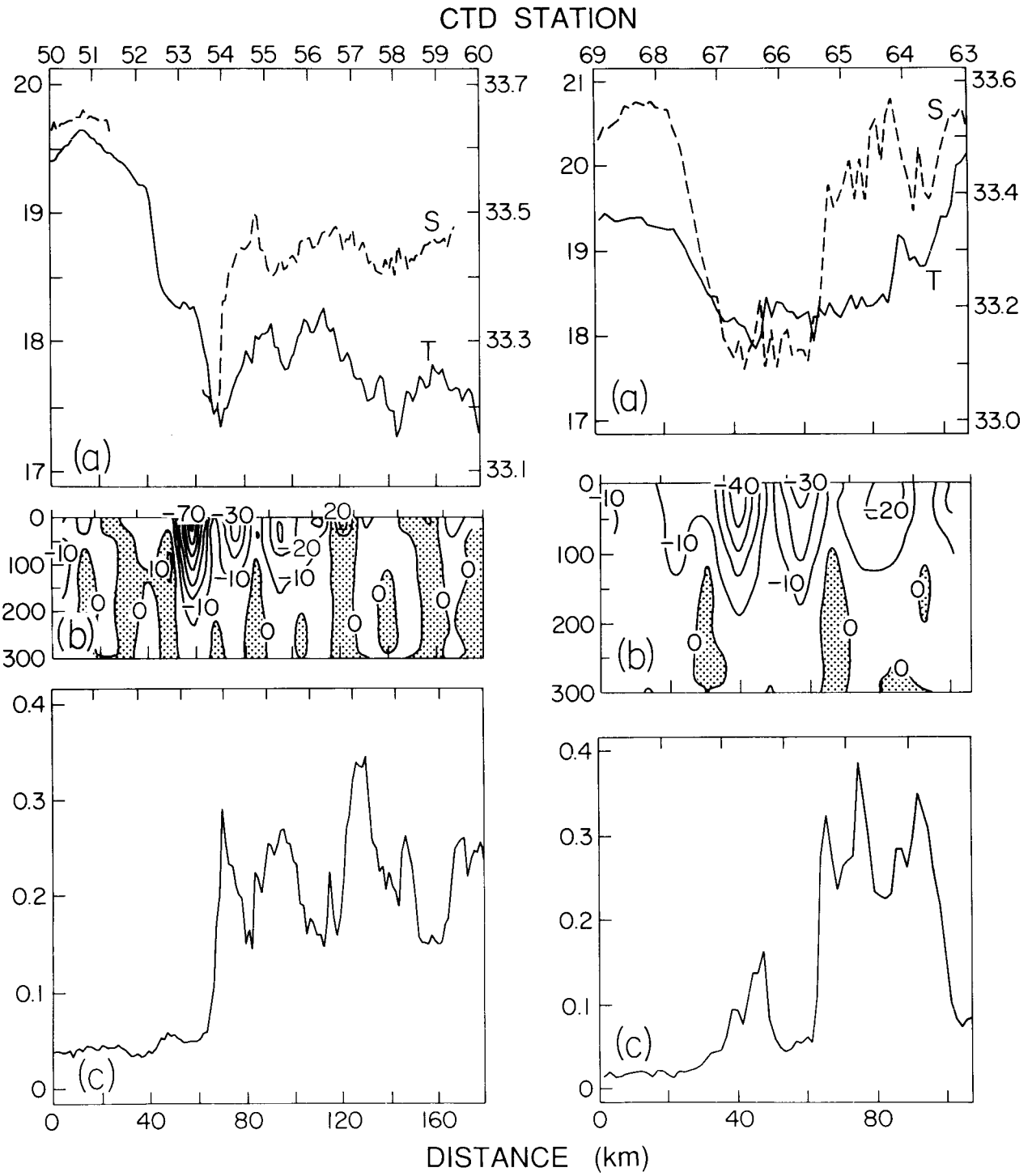

Figure 5. *a*, Surface (3-m) temperature (°C) and salinity (psu); *b*, geostrophic currents relative to 300 db; and *c*, surface chlorophyll (μg l $^{-1}$) for two sections (CTD stations 50–60 and 63–69; figure 1a) across the shoreward-flowing jet during FRONTS 85 Leg I. Northwestward flow is indicated by *stippling*. Note that the high chlorophyll peaks are associated with the high-gradient regions between the cores of the filaments.

31° 20′N, 121° 40′W) forming the southwestern portion of the front (figure 3).

Comparisons of the averaged physical properties and other physical characteristics at the terminal stations of the three sections are presented in table 2.

The W-E transect that followed the N-S sections (figure 1b) had narrower station spacing (20 km) except for the two easternmost stations (50 km). From the profiles obtained (figure 11), it is apparent that the section ran from the western side of the

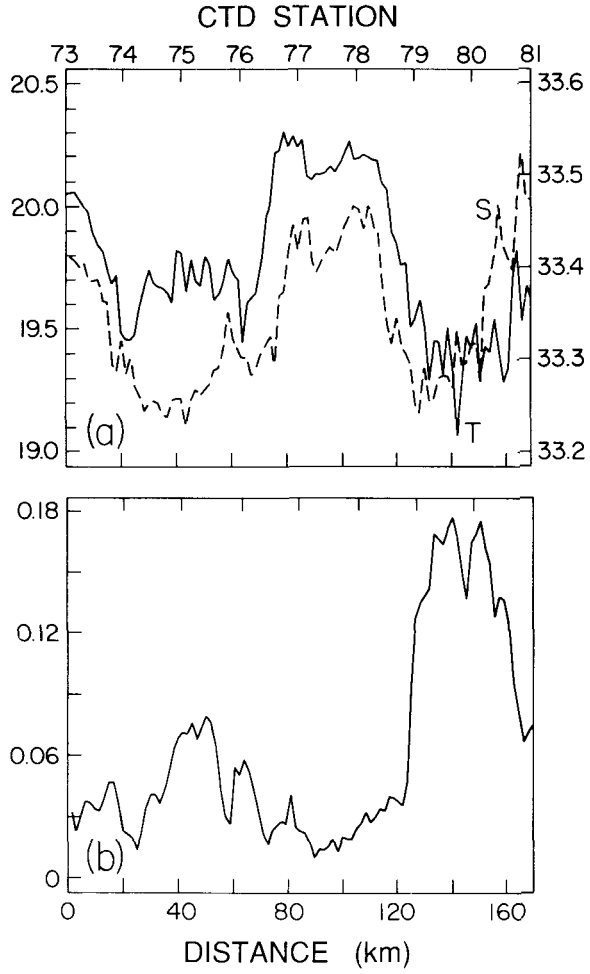

Figure 6. *a*, Surface temperature (°C) and salinity (psu), and *b*, surface chlorophyll ($\mu g\ l^{-1}$) from the easternmost section (stations 73–81; figure 1a) across the shoreward-flowing jet. The strong filaments seen in figure 5 have weakened and dispersed.

southward-flowing filament into the region of warm water (>19°C) nearer the coast. The peak southward velocity of more than 40 cm s^{-1} occurred to the east (between stas. 31 and 32) of the preceding N-S transects, again evidence that the southward filament may have drifted eastward during Leg II.

The infrared image (figure 3) shows the eastern edge of the filament broken up into smaller jets, much like the structure of the shoreward-flowing portion of the filament (figure 5). Evidence for this is seen in the hydrographic section (figure 11) between stations 30 and 33 and in the underway surface temperature (figure 12).

Biology

Underway chlorophyll fluorescence and seven primary-production stations (with nutrient and chlorophyll/phaeophytin profiles to the 0.4% light level) were the only biological measurements made on Leg I (see figure 1b). Therefore the main focus of the following discussion is on the Leg II sections.

Nutrients. The N-S and W-E nutrient sections for nitrate, nitrite, phosphate, and silicate are shown in figures 8 and 11. The transition between a nutricline depth of about 35 m to the north and 100 m to the south (table 2) was gradual over the first two transects. The last transect, however, appears to have a higher horizontal gradient between stations 20 and 23, another indication that this section ran closer down the center of the filament than did the previous two, as suggested by the physical data (see above). On the W-E transect, the nutricline shoaled to the east to a similar depth as that at the north end

TABLE 2

Comparisons of Averaged Properties at Stations North and South of the Ensenada Front, and Single Values at the Ends of the West-to-East Transect (Figure 1)

	North sta. 10, 26	South sta. 2, 8	N/S ratio	West sta. 28	East sta. 37
Surface temp. (°C)	16.6	19.0		16.8	19.0
Surface salinity (psu)	33.32	33.57		33.32	33.65
Salinity minimum (psu)	33.23	32.28		33.20	33.42
Salinity min. depth (m)	43	96		63	42
Mixed-layer depth (m)	~25	~25		~25	~20
Nutricline depth (m)	~35	100		70	32
Surface Chl. *a* ($\mu g/l$)	0.17	0.09		0.32	0.16
Deep Chl. max., DCM ($\mu g/l$)	0.35	0.23		0.36	0.74
DCM depth (m)	51	100		22	42
Integr. Chl. *a*, 0–200 m (mg/m^2)	23	23	1.0	31	30
Primary production ($mg/m^2/exp$)	604	230	2.6	—	—
Zoopl. biomass 0–210 m day ($ml/1000\ m^3$)	335	117	2.9	133	89
Zoopl. biomass 0–210 m night ($ml/1000\ m^3$)	474	149	3.2	—	—
Zoopl. biomass night/day ratio	1.4	1.3		—	—

Zooplankton biomass (wet displacement volume) from oblique net tows to 210 m.

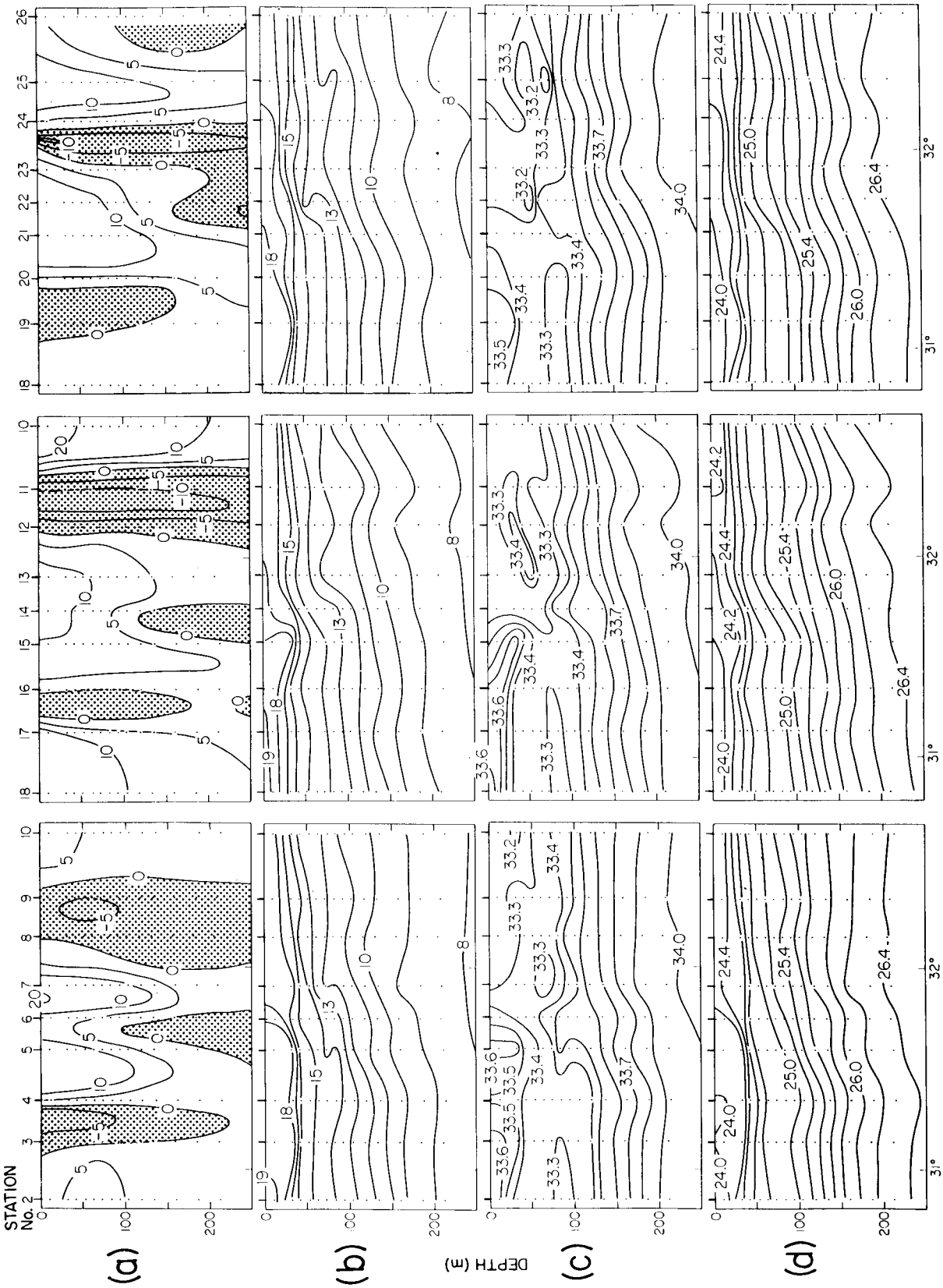

Figure 7. Hydrographic sections across the Ensenada Front from the three transects made on FRONTS 85 Leg II. *Left column*, stations 2–10 (0907 LT, 14 July to 0742 LT, 16 July); *center*, stations 10–18 (0306 LT, 17 July to 0724 LT, 18 July); *right column*, stations 18–26 (0203 LT, 19 July to 0134 LT, 21 July). *a*, Geostrophic velocity (cm s^{-1}); negative (*stippled*) velocity indicates westerly flow; *b*, temperature (°C); *c*, salinity (psu); and *d*, density (σ_θ).

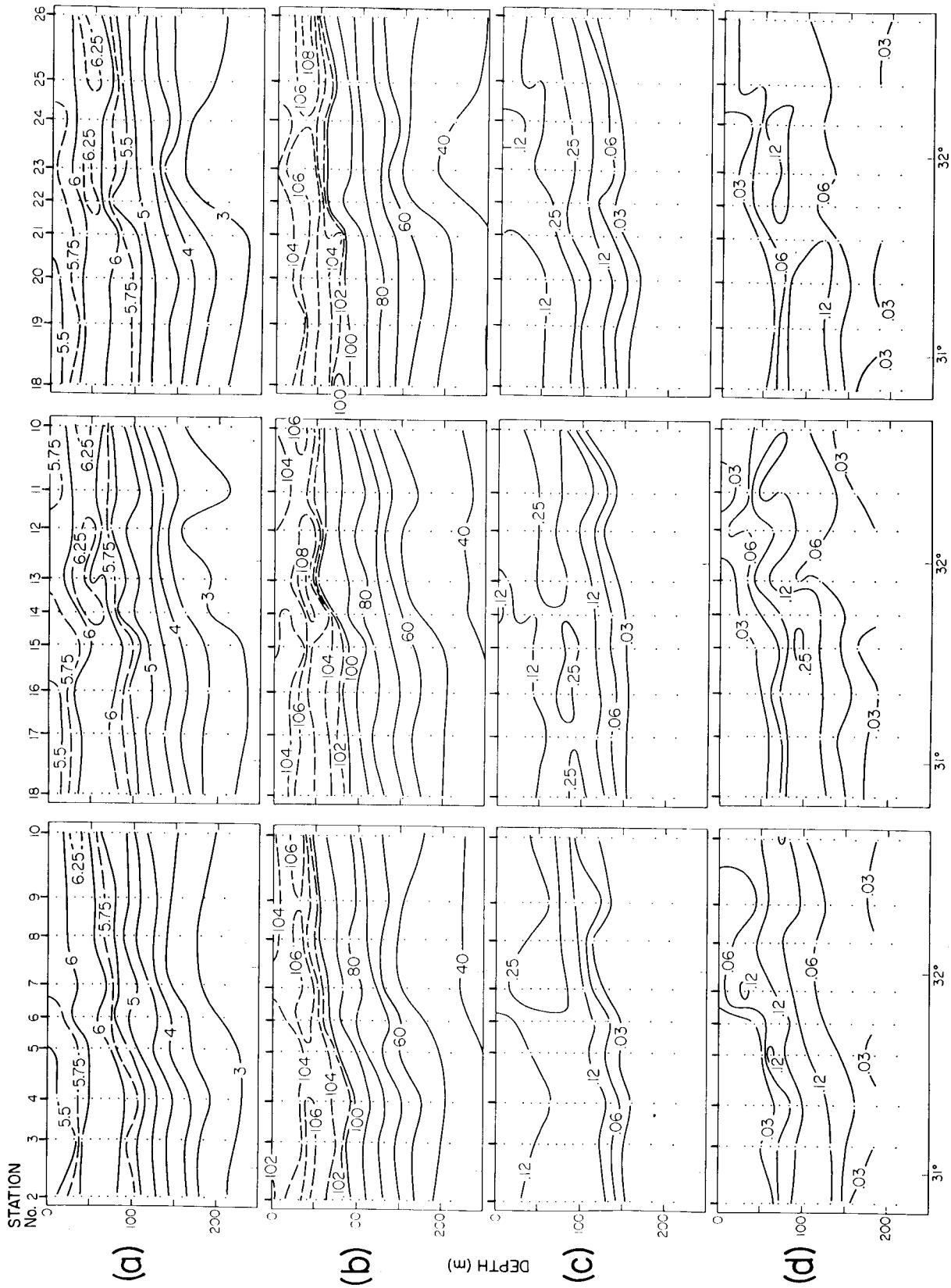

Figure 8. Similar to figure 7, except that a indicates oxygen (ml l^{-1}); *b*, oxygen saturation (%); *c*, chlorophyll *a* (µg l^{-1}); and *d*, phaeophytin (µg l^{-1}).

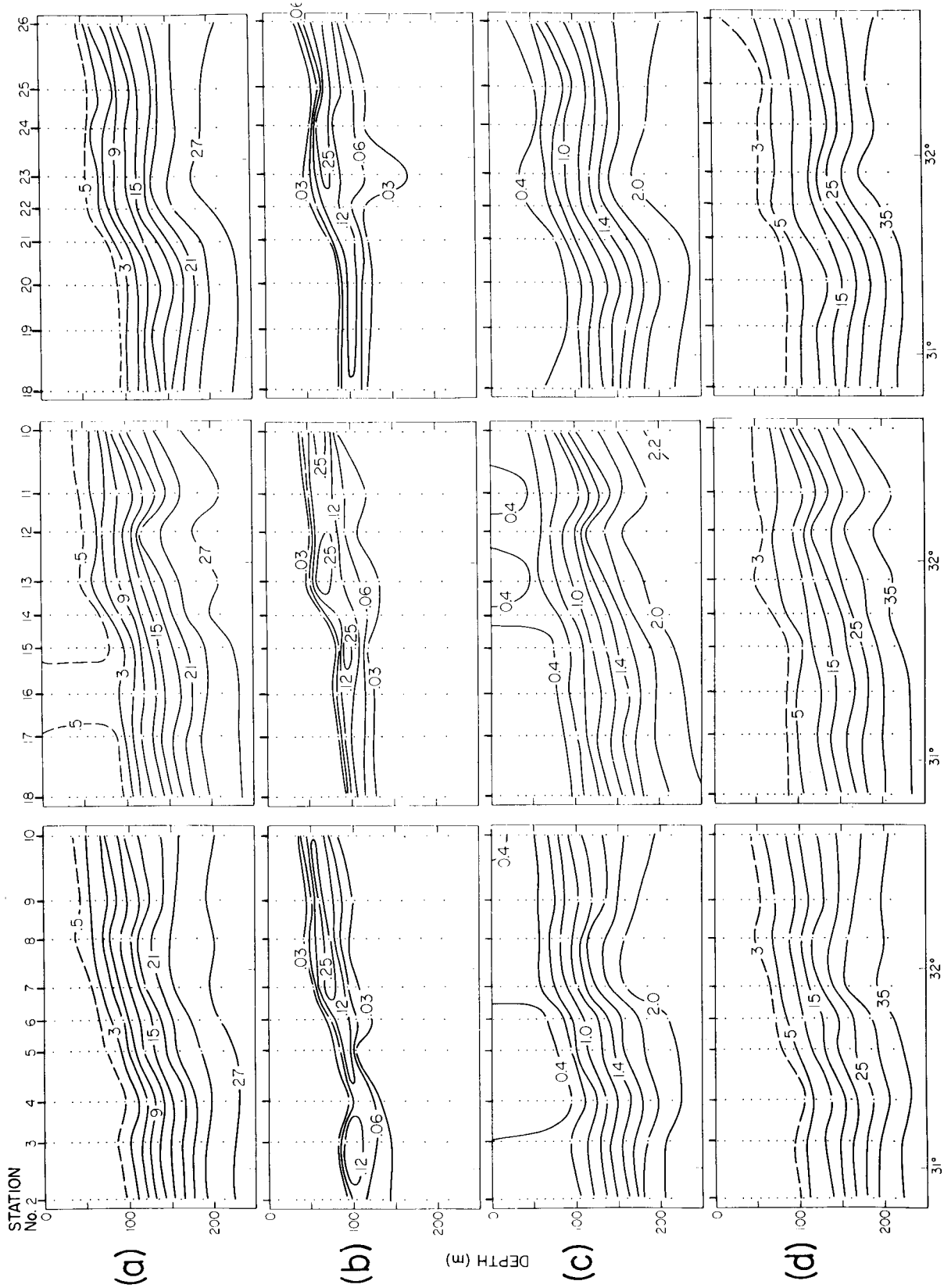

Figure 9. Similar to figure 7, except that a indicates nitrate; *b*, nitrite; *c*, phosphate; and *d*, silicate (all units $\mu M\ l^{-1}$).

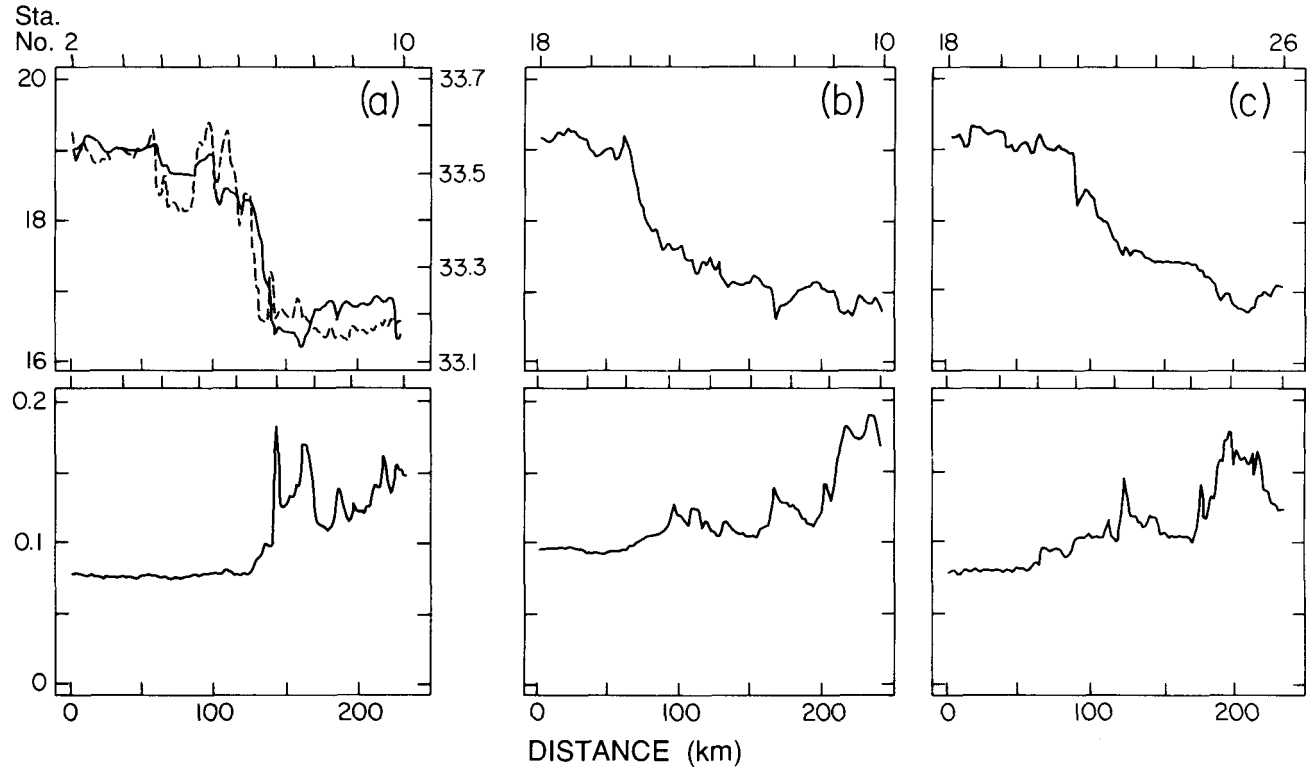

Figure 10. Underway measurements of near-surface temperature (°C) and chlorophyll (μg l^{-1}) on the three north-south transects across the Ensenada Front (figure 1b). *a*, section 1, stations 2–10; *b*, section 2, stations 10–18; *c*, section 3, stations 18–26. See figure 7 for times and dates. Salinity values (psu; *dashed line*) for the first section (stations 2–10) are overlaid on the temperature trace.

of transects 1–3; the vertical gradient in the nutricline was much greater, however, so that equivalent deeper values were about 50 m shallower to the east than to the north. The transition from west to east occurred abruptly at the thermohaline front between stations 31 and 32, marking the eastern edge of the southward-flowing filament.

Chlorophyll and primary production. The vertical distributions of chlorophyll and phaeophytin obtained from the Leg II sections are shown in figures 8 and 11. Of note in these sections are the general low gradients in chlorophyll/phaeophytin in the N-S sections and the strong gradient in the W-E section. Plots of integrated chlorophyll over the depth of sampling as a function of station position (figure 13) show how this results in no change in chlorophyll standing stock in the N-S direction, whereas the strong deep chlorophyll maximum (figure 11 and table 2) under the warm waters to the east yields a larger average standing stock than in the north or west.

Surface chlorophyll fluorescence measured under way on Leg I is mapped in figure 4d; primary production integrated over the euphotic zone from both legs is mapped in figure 4e. Chlorophyll in the surface waters of the filament appears to decrease by a factor of about three during the transit through the study area. Primary production, although there is a strong NE-to-SW gradient, does not appear to be enhanced in the filament waters.

Table 2 shows that the production was approximately three times greater to the north of the front, yet the standing crop of chlorophyll was similar on both sides (see also figure 13), as were the assimilation numbers of the phytoplankton (Gaxiola-Castro and Alvarez-Borrego 1991). The vertical distributions of chlorophyll with respect to the 1% light level and the nutricline (defined as the depth where NO_3 reaches 0.5 μM) are shown in figure 14.

Comparisons of the patterns of chlorophyll and primary production with temperature and geopotential anomaly show a general broad agreement in overall form, but differences in detail (figure 4). The northeast-southwest gradient from high to low values of chlorophyll and primary production reflects the boundary formed by the southeastward flowing jet (figure 4a). Higher values of chlorophyll (>0.4 μg l^{-1}) correspond better to regions with geopotential anomalies of less than about 5.4 m^2s^{-2} than they do to cold temperatures. The highest values of primary production (806 mgC m^{-2} exp^{-1}), chlorophyll (>1.5 μg l^{-1}), and chlorophyll gradients correspond

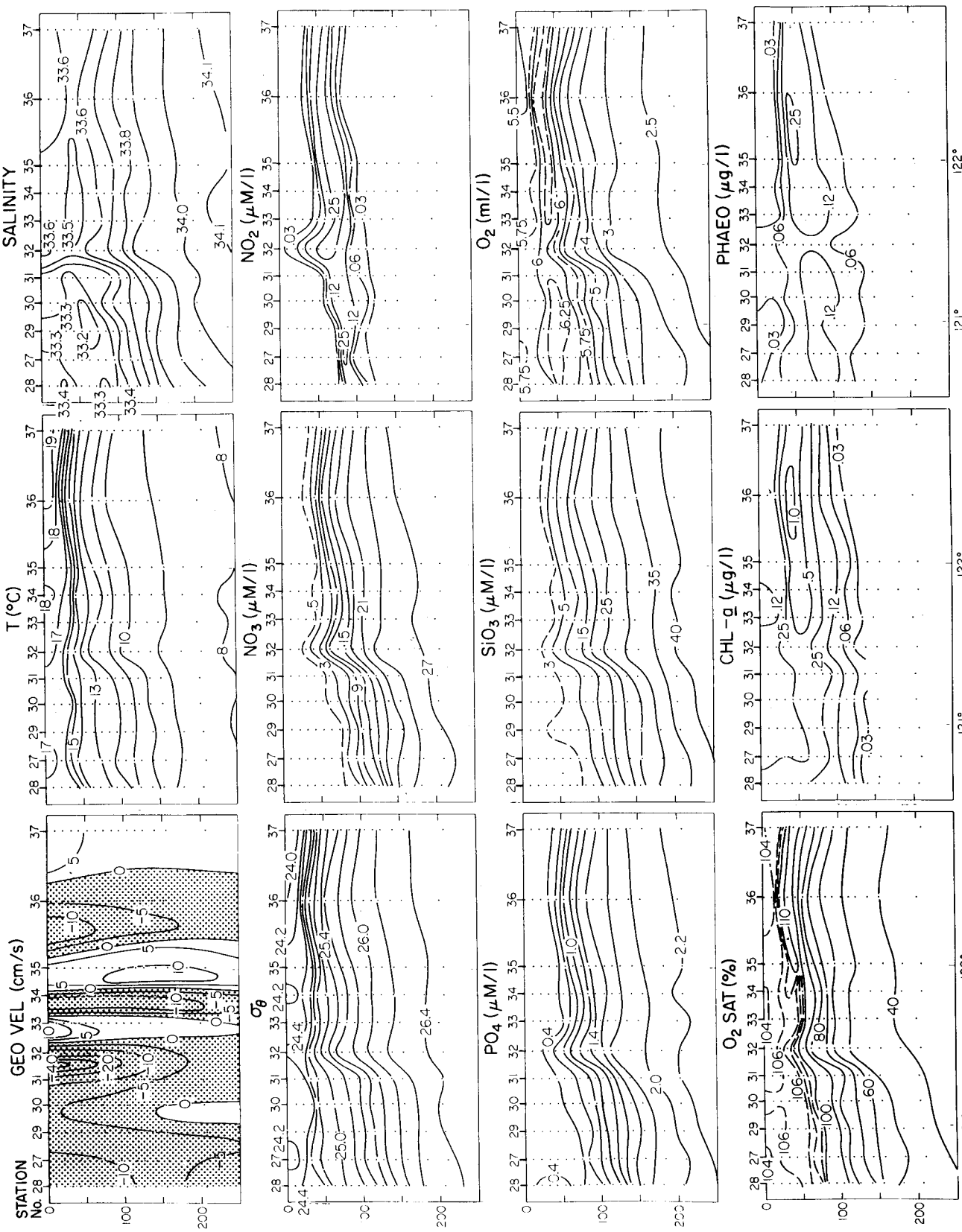

Figure 11. Hydrographic section perpendicular to the three north-south sections shown in figures 7–9 at stations 28–37, 1045 LT, 21 July, to 1639 LT, 22 July. Negative (*stippled*) velocity indicates southerly flow.

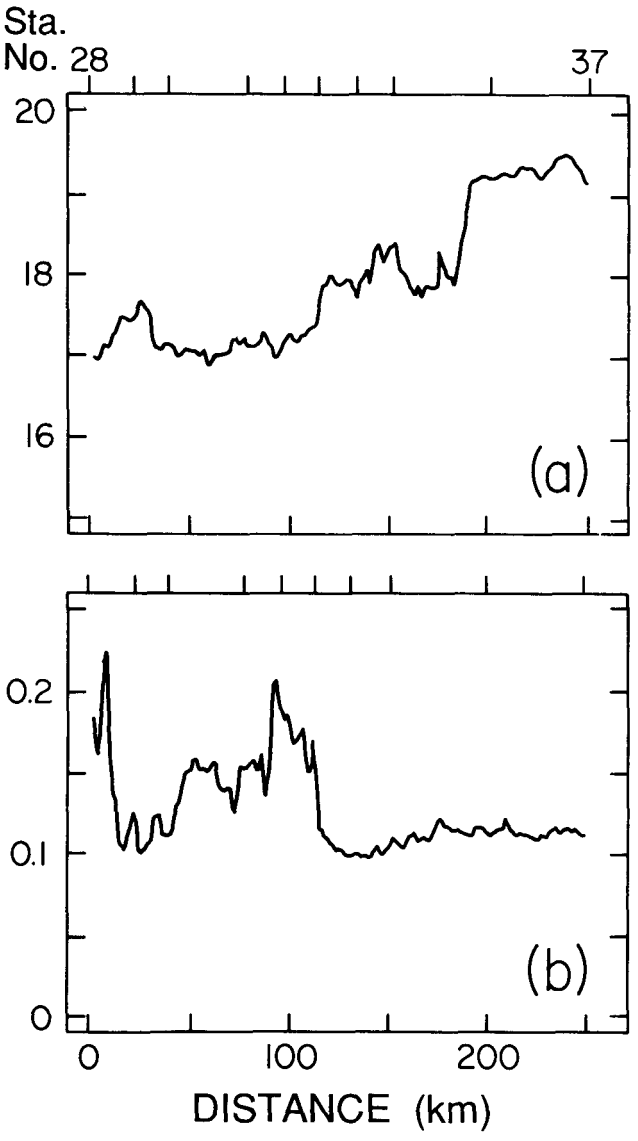

Figure 12. Underway measurements of *a*, near-surface temperature (°C) and *b*, chlorophyll ($\mu g\ l^{-1}$) on the west-to-east transect shown in figure 11.

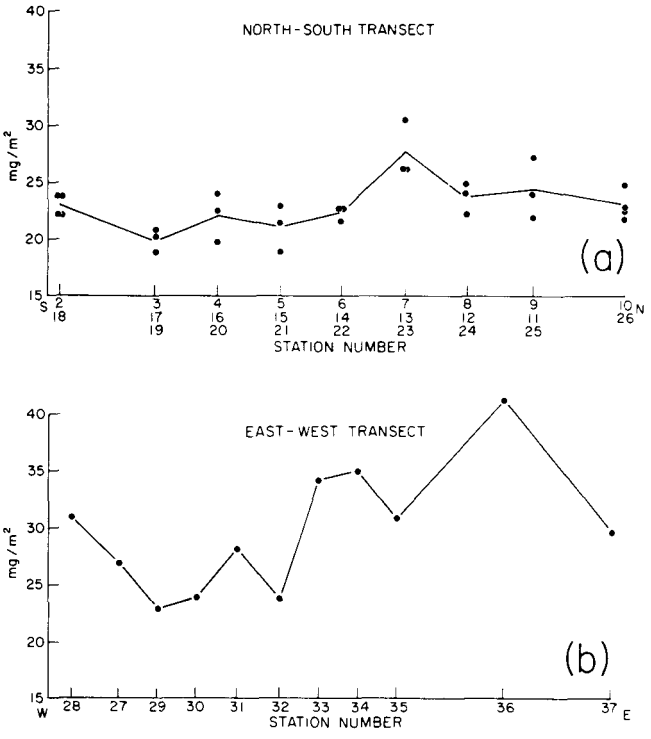

Figure 13. Integrated chlorophyll along the north-south (*a*) and east-west (*b*) transects. The *solid lines* connect the average values for the data at each station.

to the lowest geopotential anomaly ($<5.2\ m^2s^{-2}$) in the northeast corner of the survey area, but this region is also associated with shallow topography in the vicinity of San Nicholas Island and with a warm-water intrusion from the east (figure 4c). The N-S-trending ridge of high positive divergence ($>3\times10^{-7}s^{-1}$) in the middle of the study area (figure 4b) approximately follows the eastern side of the jet axis (figure 4a); surface chlorophyll in general follows this pattern, but in detail, the high-chlorophyll regions are not closely related to highs in positive divergence, as might be expected if the divergence estimate were a good measure of the biological consequences of upwelling. Productivity does not seem well matched at all.

The relationship of surface chlorophyll to the geostrophic velocities measured on the two Leg I sections across the eastward-flowing jet (figure 5) shows that the high chlorophyll values are associated with the high-velocity-gradient regions between the jets and not with the core of the jets. For example, in the first section (figure 5) the 70-cm s^{-1} jet core has a chlorophyll minimum between a slightly higher value on the south side and a sharp peak to the north. The regions between both northward- and southward-flowing components show chlorophyll peaks.

The sequence of Leg II chlorophyll sections (figure 8) shows an increasing extension of the >0.25 $\mu g\ l^{-1}$ subsurface maximum to the south, lending support to the suggestion that the sections were progressively closer to the axis of the southward-flowing filament. This may also indicate the consequences of the subduction of the southward-flowing waters that is suggested by the layer of lower-salinity water. The extent of the low salinity (and other nutrients) did not differ much between the sections to the south of the front, but the chlorophyll definitely was greater. Perhaps the third section passed down the core of the subducting water. The Leg II measurements of surface chlorophyll fluorescence (figure 10) also show an extension of high chloro-

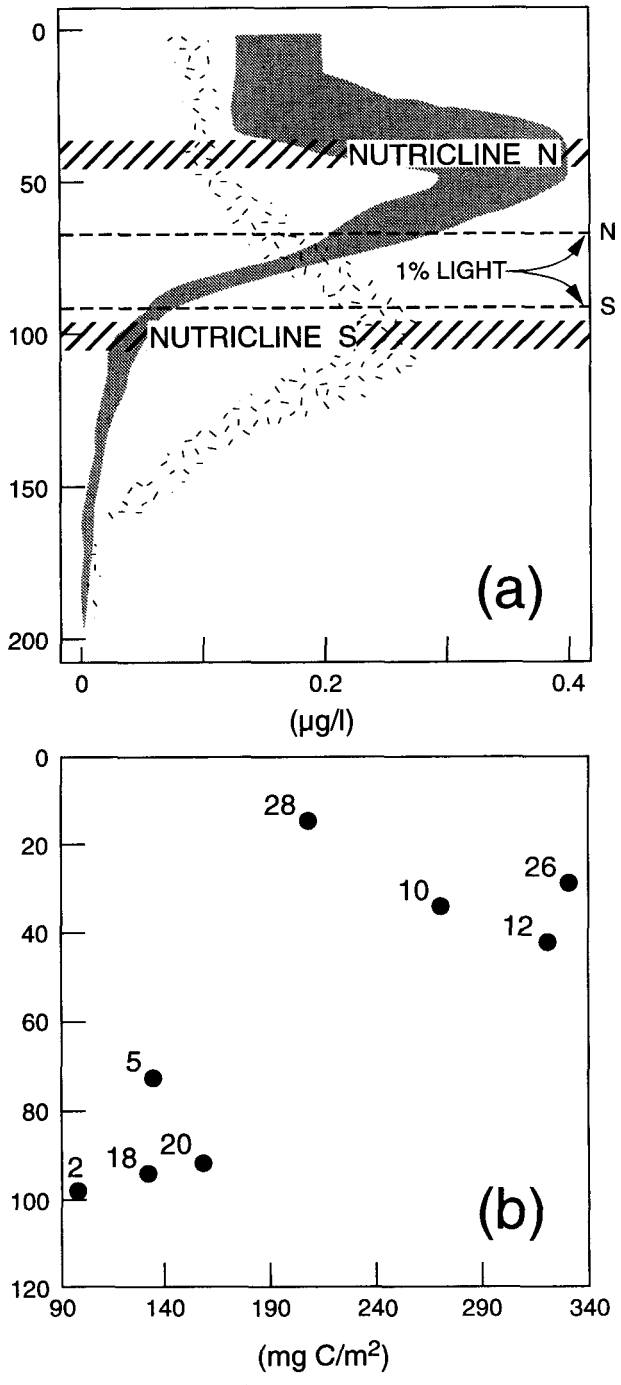

Figure 14. *a*, Depth (m) profiles of chlorophyll (μg l^{-1}) from all casts taken at the northern stations (10, 26; *shaded*) and southern stations (2, 18; *stippled*). *b*, Primary production plotted as a function of the nutricline depth (depth where nitrate exceeds 0.5 μM). Station numbers are indicated at each point.

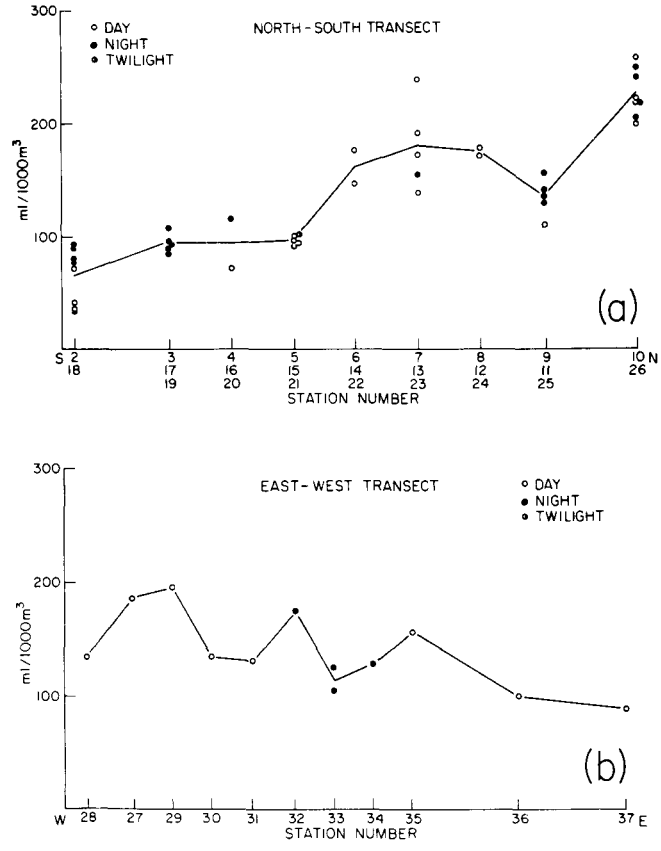

Figure 15. Macrozooplankton displacement volume in the upper 210 m along the (*a*) north-south and (*b*) east-west transects. The *solid lines* connect the average values for the data at each station.

phyll south of the front in sections 2 and 3 that is not evident in section 1.

Although the chlorophyll profile of the W-E section (figure 11) shows little detail in the upper 20 m, there is rich pattern in the underway measurements of surface chlorophyll fluorescence (figure 12).

There are also interesting similarities to the structure observed in the three N-S sections from Leg I. Comparison of the fluorescence section (figure 12) with the geostrophic velocity section (figure 11) shows that the high chlorophyll values between stations 32 and 33 are associated with the high shear region east of the strong (>40 cm s^{-1}) southward flow and with the western edge of the northward filament. The relatively strong (>10 cm s^{-1}) and warm (>18°C) southward filament near station 34 had the lowest surface chlorophyll (<0.12 μg l^{-1}) of the eastern half of the section. The westernmost southward flow of >10 cm s^{-1} was also warmer (>17.5°C) and associated with chlorophyll values of <0.12 μg l^{-1}; this feature appears to be the anticyclonic intrusion of warmer water from the west seen in the vicinity of 32°N 121°W.

Zooplankton. Zooplankton biomass (displacement volume, including fish eggs and larvae) integrated over the upper 210 m for the N-S and W-E sections is plotted in figure 15. The northernmost station is characterized by a biomass about three times higher than that of the southern terminal station (table 2). The break between the high biomasses of the north

and lower biomasses in the south occurs abruptly between stations 5/15/21 and 6/14/22, a distance of about 13 km; this is the region of the front with the highest gradients in other properties (figures 7–10). The W-E section shows a general decrease of zooplankton biomass to the east beyond station 28; this station appears to have been taken in the warmer waters to the west of the filament.

Zooplankton biomass in the upper 210 m of the water column from the N-S sections varied directly with integrated chlorophyll, while that from the W-E section varied inversely (figure 16). The variation in the W-E section is due to the transition from a western, weakly stratified water column with low integrated chlorophyll and relatively high zooplankton biomass, to highly stratified waters with a strong DCM overlaid by zooplankton-poor waters in the east. The macrozooplankton day-night displacement-volume ratio of about 1.4 (table 2) both north and south of the front suggests a similar day-night difference in grazing pressure on the phytoplankton.

The day and night vertical distributions of zooplankton biomass (displacement volume) over the upper 1000 m of the water column at the north and south terminal stations of the sections are presented in figure 17. These distributions clearly show the increased biomass at all depths at the northern station, both day and night. The concentration of the highest biomasses in the upper 100 m results in north/south biomass ratios between the upper 100 m of the terminal stations of 4.2 for night, and 3.8 for day, as compared to 3.2 and 2.9 for the 210-m integrating bongo tows (table 2).

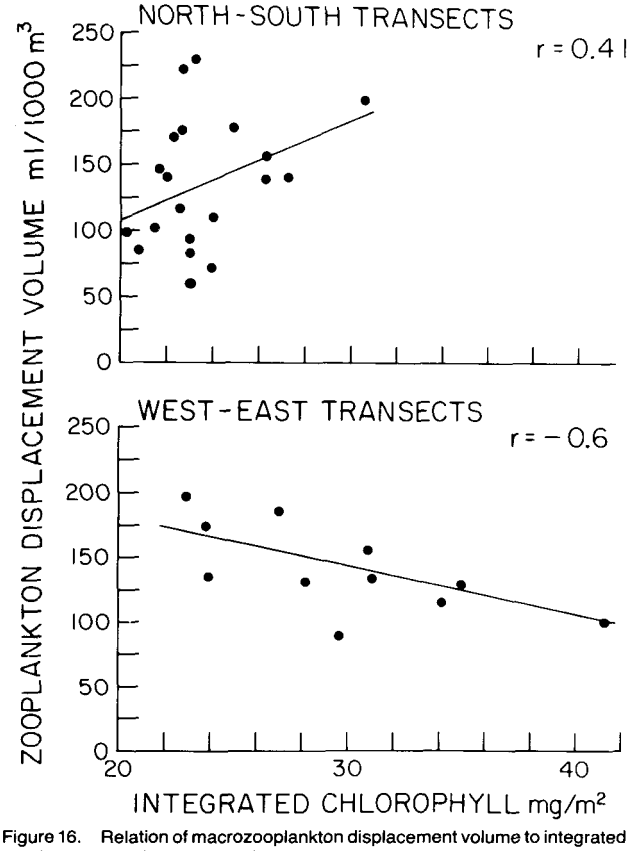

Figure 16. Relation of macrozooplankton displacement volume to integrated chlorophyll on the north-south and west-east transects.

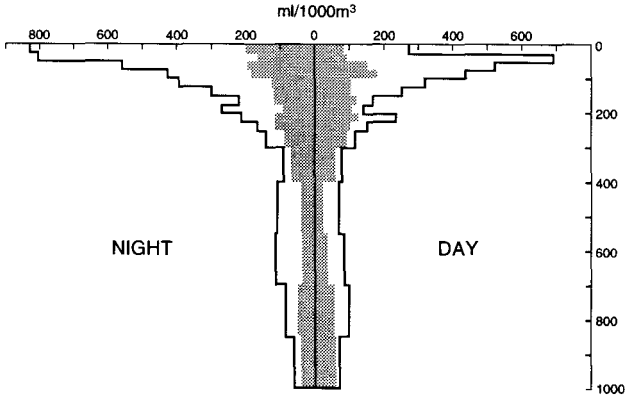

Figure 17. Vertical profiles (depth in meters) of day and night zooplankton biomass (wet-displacement volume) to the north (stations 10, 26; *solid lines*) and south (stations 2, 18; *shaded*) of the Ensenada Front. The values shown are the averages of two samples taken at each depth. At the northern station, a layer of abundant detrital material (flocculent aggregates and large fecal pellets) was present between 400 and 850 m, with a peak at about 600 m.

At the northern stations below about 400 m, biomass increased slightly with depth to peaks at 550–700 m during the night and 700–850 m during the day; a small fraction (unmeasured) of this was due to a layer of grey-green flocculent organic aggregates and large fecal pellets, similar to those of salps, between 400 and 850 m. The peak abundance of this material was about 600 m. No such feature was noted for the southern stations.

Total fish eggs and larvae counted in the net samples describe the way that ichthyoplankton varies across the front and in its vertical distributions at the terminal stations of the sections. Figure 18 presents the results from the 210-m integrating bongo net tows along each of the four sections. Except for the samples collected at station 2 (figure 18a), both eggs and larvae in the three N-S sections decreased in abundance to the north; regressions of eggs and larvae against stations using the combined data for the three sections showed, however, that only eggs had a significant negative relationship to station position ($r = -0.63$, $p < 0.0001$). On the W-E section, the larvae decreased in abundance across the southward-flowing filament, but eggs did not (figure 18d). Regression of fish larvae against eggs from the three

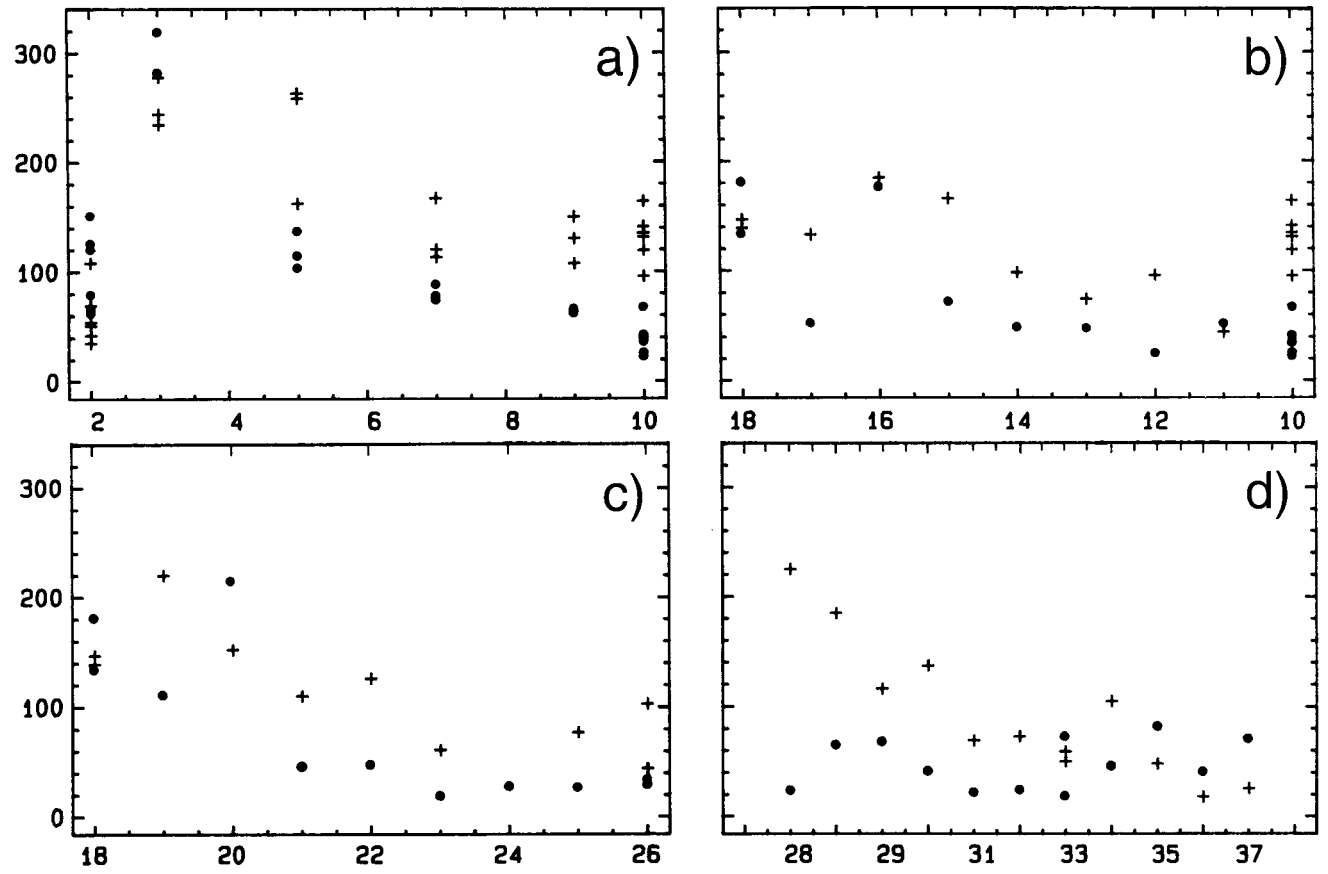

Figure 18. Abundance (numbers/1000 m³) of fish eggs (·) and larvae (+) from the 0–210-m oblique CalBOBL net tows at each station of three north-south (*a–c*) and one west-east (*d*) transects (see figure 1b); station numbers are indicated at bottom of each plot. Day values have been multiplied by 1.2 for eggs and 1.5 for larvae to correct for consistent day-night differences in abundance.

N-S sections (figure 19) showed a significant relationship between larvae and eggs ($r = 0.57$, $p < 0.0001$).

The day and night vertical distributions of fish eggs and larvae at the terminal stations are shown in figure 20. Fish eggs in the south were much more abundant than to the north, both day and night; larval abundances were about equal in both areas, except in surface waters to the north at night. Diel shifts in vertical distribution and abundance are clear only for eggs south of the front, and larvae north of the front.

DISCUSSION

Satellite imagery has shown the Ensenada Front to be one of the dominant features of the California Current off southern California and northern Baja California (Pelaez and McGowan 1986; Strub et al. 1990; Thomas and Strub 1990). Many large-scale oceanographic surveys, especially the CalCOFI program, have covered the area of the frontal system, but few have focused enough on the frontal area to provide detailed physical, biological, and chemical information on the nature of the frontal system. The ship-tracked drogue measurements of Reid et al. (1963) confirmed the shoreward sweep of surface waters and revealed the mesoscale eddies associated

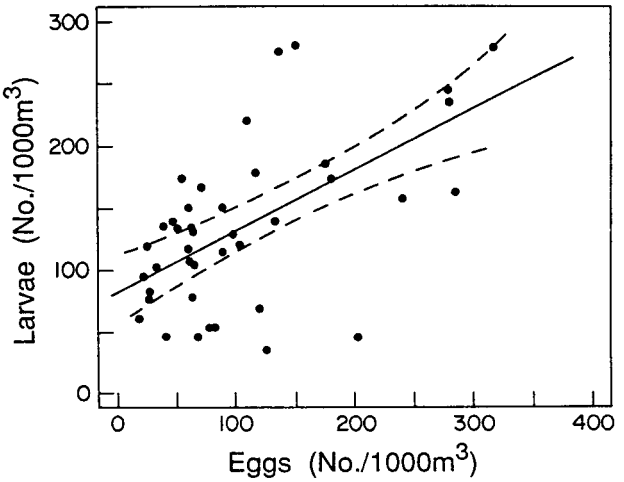

Figure 19. Regression of total fish larvae on total fish eggs for all 0–210-m oblique CalBOBL net tows taken on FRONTS 85 Leg II. *Dashed lines* are the 95% confidence intervals.

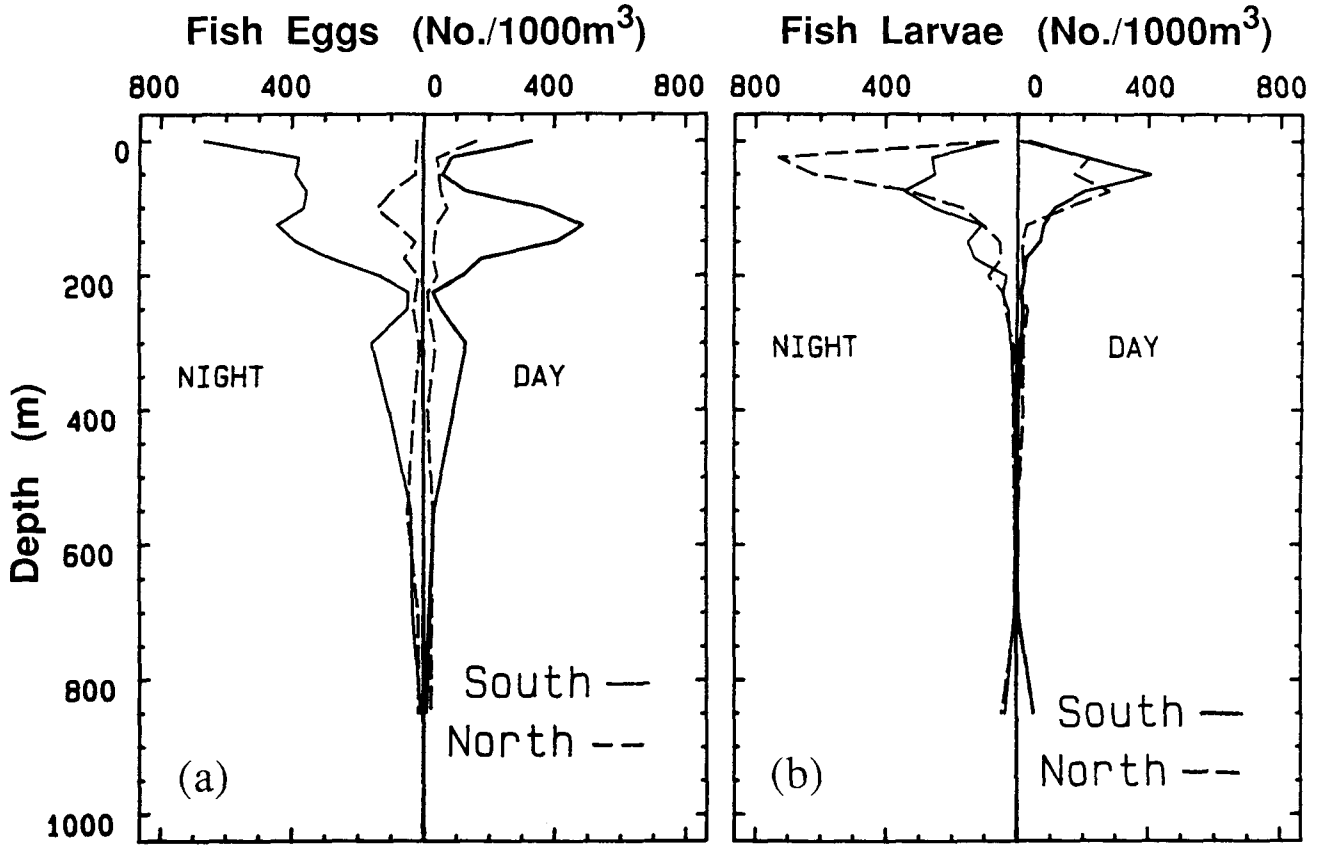

Figure 20. Vertical profiles of abundance of *a*, all fish eggs and *b*, all fish larvae from the MOCNESS samples taken to the north (stations 10, 26; *dashed lines*) and south (stations 2, 18; *solid lines*) of the Ensenada Front. The values shown are the averages of two samples taken at each depth.

with the flow. A study by Simpson and Lynn (1990), nearly contemporaneous with the one described here, surveyed the same area but reported primarily on the mesoscale eddy dipole to the northwest of our study area.

The flow within our study area, localized within a narrow, intense filament forming only a small part of the large-scale classical picture of the southward-flowing California Current, transports a volume of water (relative to 300 db) comparable to that calculated on the basis of much larger areal averages (Bernal and McGowan 1981; Haury and Shulenberger 1982). Its transport is similar to that of the equatorward jet off northern California surveyed by Huyer et al. (1991). It also transports volumes of the same order as those of offshore-directed jets (Flament et al. 1985; Washburn and Armi 1988).

The large volume of water transported by the filament is relatively rich in chlorophyll and zooplankton. When this water exits the filament system by entering the Southern California Bight or the numerous eddies to the south and east, much of the biological richness has disappeared. The biological and physical mechanisms for the changes observed are not well understood. Some fraction of these waters appears to be subducted beneath the warm, oligotrophic waters to the south of the front. Whether this is an important mechanism for the loss of organic material from the California Current is the subject of continuing study.

Also not understood is the nature of the processes contributing to the relative richness of the filament waters. Advection from upwelling centers and other loci of enrichment processes to the north may contribute most of the nutrients and organisms, but the complexity of the flow structure in the filament may be a significant *in situ* source. For example, enhanced vertical mixing should result from the large shears between the multiple "strands" of the filament revealed by the CTD and hydrographic sections (figures 5, 7, 11) and satellite imagery (figure 3). Interactions between the wind field and these small-scale velocity structures can also cause upwelling and downwelling (Paduan and Niiler 1990; Lee et al., in press). The enhanced chlorophyll in these high-shear zones (figure 5) seen in the underway measurements suggests that enrichment or convergence does occur.

Thomas and Strub (1990), using CZCS imagery from 1981, have shown the seasonal character of the surface manifestations of the Ensenada Front (their figure 3). Our chlorophyll values from the underway measurements (figures 5, 6, 10) and from surface bottles of the hydrographic sections (figure 8) agree both in quantity and in the position of the frontal region between 31° and 32.5°N during the summer period. As Thomas and Strub (1990, p. 13,036) caution, however, the near-surface values do not well represent the water column biomass; this is graphically illustrated by comparing our figures 7–10 to the integrated chlorophyll value from the sections (figure 13a). There is clearly no front evident in the water-column-averaged standing crop of phytoplankton.

ACKNOWLEDGMENTS

We thank the following for invaluable assistance: our Mexican colleagues at CICESE, the Instituto Nacional de Pesca, and the Secretaria de Marina for their participation in the cruise; Arnold Mantyla for checking and contouring the hydrographic sections; Sarilee Anderson for providing the geostrophic velocity sections in figures 7 and 11; the technical staff of MLRG for collecting data at sea—particularly Cecilia Kemper for collecting the chlorophyll and productivity data from Leg I, George Anderson for analyzing the nutrients, and Jim Schmitt for running the MOCNESS. We also thank Geoff Moser and Paul Smith of the National Marine Fisheries Service, Southwest Fisheries Science Center, for the data on fish eggs and larvae. Guy Tapper and Nancy Hulbirt of the MLRG graphics department prepared the illustrations. This study was supported in part by Office of Naval Research contract N00014-89-J-1116.

LITERATURE CITED

Bernal, P., and J. McGowan. 1981. Advection and upwelling in the California Current. *In* Coastal upwelling, F. A. Richards, ed. American Geophysical Union, pp. 381–399.

Bernstein, R. L., L. Breaker, and R. Whritner. 1977. California eddy formation: ship, air and satellite results. Science 195:353–359.

Brinton, E. 1976. Population biology of *Euphausia pacifica* off southern California. Fish. Bull. 74:733–762.

Flament, P., L. Armi, and L. Washburn. 1985. The evolving structure of an upwelling filament. J. Geophys. Res. 90:11,765–11,778.

Gaxiola-Castro, G., and S. Alvarez-Borrego. 1991. Relative assimilation numbers of phytoplankton across a seasonally recurring front in the California Current off Ensenada. Calif. Coop. Oceanic Fish. Invest. Rep. 32:91–96.

Haury, L., and E. Shulenberger. 1982. Horizontal transport of phosphorus in the California Current. Calif. Coop. Oceanic Fish. Invest. Rep. 13:149–159.

Haury, L., J. McGowan, E. Brinton, P. Walker, C. Fey, and A. Townsend. 1990. Distribution of zooplankton biomass/species and fish eggs/larvae across the Ensenada Front in 1985. EOS 71:147.

Haury, L. R., P. M. Poulain, A. W. Mantyla, E. L. Venrick, and P. P. Niiler. 1986. FRONTS cruise, data report, SIO Ref. 86-23, Scripps Inst. Oceanogr., Univ. Calif., San Diego.

Hickey, B. M. 1979. The California Current system—hypotheses and facts. Prog. Oceanogr. 8:191–279.

Huyer, A., P. M. Kosro, J. Fleischbein, S. R. Ramp, T. Stanton, L. Washburn, F. P. Chavez, T. J. Cowles, S. D. Pierce, and R. L. Smith. 1991. Currents and water masses of the coastal transition zone off northern California, June to August 1988. J. Geophys. Res. 96: 14,809–14,831.

Jackson, G. A. 1986. Physical oceanography of the Southern California Bight. *In* Plankton dynamics of the Southern California Bight, R. W. Eppley, ed. Lecture notes on coastal and estuarine studies, 15. Springer-Verlag, pp. 13–52.

Kramer, D., M. J. Kalin, E. G. Stevens, J. R. Thrailkill, and J. R. Zweifel. 1972. Collecting and processing data on fish eggs and larvae in the California Current region. NOAA Tech. Rep. NMFS CIRC-370, 38 pp.

Lee, D. K., P. Niiler, A. Warn-Varnas, and S. Piacsek. In press. Wind driven secondary circulation in ocean mesoscale. J. Mar. Res.

Legeckis, R. 1978. A survey of the world wide sea surface temperature fronts detected by environmental satellites. J. Geophys. Res. 83: 4501–4522.

Lynn, R. J. 1986. The subarctic and northern subtropical fronts in the eastern North Pacific Ocean in spring. J. Phys. Oceanogr. 16: 209–222.

Lynn, R. J., and J. J. Simpson. 1987. The California Current system: the seasonal variability of its physical characteristics. J. Geophys. Res. 92:12,947–12,966.

Moser, H. G., and P. E. Smith. In press. Larval fish assemblages of the California Current and its associated water masses. Proc. Los Angeles County Museum of Natural History, Science Series.

Niiler, P. P., R. E. Davis, and H. J. White. 1987. Water-following characteristics of a mixed layer drifter. Deep-Sea Res. 34:1867–1882.

Niiler, P. P., P. M. Poulain, and L. R. Haury. 1989. Synoptic three-dimensional circulation in an offshore-flowing filament of the California Current. Deep-Sea Res. 36:385–405.

Paduan, J. D., and P. P. Niiler. 1990. A Lagrangian description of motion in northern California coastal transition filaments. J. Geophys. Res. 95:18,095–18,109.

Pares-Sierra, A., and J. J. O'Brien. 1989. The seasonal and interannual variability of the California Current system: a numerical model. J. Geophys. Res. 94:3159–3180.

Pelaez, J., and J. A. McGowan. 1986. Phytoplankton pigment in the California Current as determined by satellite. Limnol. Oceanogr. 31:927–950.

Reid, J. L., Jr., R. A. Schwartzlose, and D. M. Brown. 1963. Direct measurements of a small surface eddy off northern Baja California. J. Mar. Res. 21:205–218.

Saur, J. F. T. 1980. Surface salinity and temperature on the San Francisco-Honolulu route June 1966–December 1970 and January 1972–December 1975. J. Phys. Oceanogr. 10:1669–1680.

Sette, O., and E. H. Ahlstrom. 1948. Estimates of abundances of the eggs of the Pacific pilchard (*Sardinops caerulaea*) off Southern California during 1940 and 1941. J. Mar. Res. 7:511–542.

Simpson, J. J. 1985. Air-sea exchange of carbon dioxide and oxygen induced by phytoplankton: methods and interpretation. *In* Mapping strategies in chemical oceanography, A. Zirino, ed. Pp. 409–449.

Simpson, J. J., and R. J. Lynn. 1990. A mesoscale eddy dipole in the offshore California Current. J. Geophys. Res. 95:13,009–13,022.

Strub, P. T., C. James, A. C. Thomas, and M. R. Abbott. 1990. Seasonal and nonseasonal variability of satellite-derived surface pigment concentration in the California Current. J. Geophys. Res. 95:11,501–11,530.

Sverdrup, H. U., and R. H. Fleming. 1941. The waters off the coast of southern California, March–July 1937. Scripps Inst. Oceanogr. Bull. 4:261–387.

Thomas, A. C., and P. T. Strub. 1990. Seasonal and interannual variability of pigment concentrations across a California Current frontal zone. J. Geophys. Res. 95:13,023–13,042.

Venrick, E. R. 1990. Behind a front: an overview of the Ensenada Front program. EOS 71:148.

Washburn, L., and L. Armi. 1988. Observations of frontal instabilities on an upwelling filament. J. Phys. Oceanogr. 18:1075–1092.

Wiebe, P. W., A. W. Morton, A. M. Bradley, R. H. Backus, J. E. Craddock, V. Barber, T. J. Cowles, and G. R. Flierl. 1985. New developments in the MOCNESS: an apparatus for sampling zooplankton and micronekton. Mar. Biol. 87:313–323.

Wyllie, J. G. 1966. Geostrophic flow of the California Current at the surface and at 200 m. Calif. Coop. Oceanic Fish. Invest. Atlas 4, La Jolla, Calif.